

A Monte Carlo simulation study on the wetting behavior of water on graphite surface

Xiongce Zhao*

Joint Institute for Computational Sciences and Center for Nanophase Materials Sciences,
Oak Ridge National Laboratory, Oak Ridge, Tennessee 37831, USA[†]

This paper is an expanded edition of the rapid communication published several years ago by the author (*Phys. Rev. B*, v76, 041402(R), 2007) on the simulation of wetting transition of water on graphite, aiming to provide more details on the methodology, parameters, and results of the study which might be of interest to certain readers. We calculate adsorption isotherms of water on graphite using grand canonical Monte Carlo simulations combined with multiple histogram reweighting, based on the empirical potentials of SPC/E for water, the 10-4-3 van der Waals model, and a recently developed induction and multipolar potential for water and graphite. Our results show that wetting transition of water on graphite occurs at 475-480 K, and the prewetting critical temperature lies in the range of 505-510 K. The calculated wetting transition temperature agrees quantitatively with a previously predicted value using a simple model. The observation of the coexistence of stable and metastable states at temperatures between the wetting transition temperature and prewetting critical temperature indicates that the transition is first order.

PACS numbers: 68.35.Rh, 64.70.Fx, 82.20.Wt

I. INTRODUCTION

When a fluid adsorbs on a solid surface at temperatures below its liquid-vapor critical temperature (T_c), the adsorbed film either spreads across the surface (wetting) or beads up as a droplet (nonwetting) as the pressure approaches the saturated vapor pressure P_{svp} of the fluid. Wetting transition describes the transition between those two kinds of behavior. Physically the wetting transition corresponds to the phenomena when the contact angle of the liquid drop on the surface changes from a nonzero value to zero. Analysis of wetting transition was first presented 30 years ago by Cahn [1] and Ebner and Saam. [2] They showed that if a fluid does not wet a particular surface at low temperature, then the system ought to exhibit wetting transition at some temperature T_w below T_c . In terms of adsorption isotherms, the wetting phenomenon should manifest itself as following three different patterns. (1) At temperatures below T_w , adsorption beginning with a thin film increases slightly as the pressure increases towards the saturation pressure P_{svp} . At P_{svp} the bulk vapor condenses completely, and the adsorption coverage becomes infinite. On a coverage versus pressure diagram, the adsorption isotherm reaches P_{svp} with a discontinuous jump (infinite slope). (2) In the temperature range between T_w and the prewetting critical temperature T_{pwc} , the thin film grows as the pressure increases until it jumps to a thick, liquid like film of finite thickness at some pressure less than P_{svp} . This thin-to-finite film transition or wetting transition is followed by continuous growth until condensation occurs at P_{svp} . (3) At temperatures higher than T_{pwc} , the film grows con-

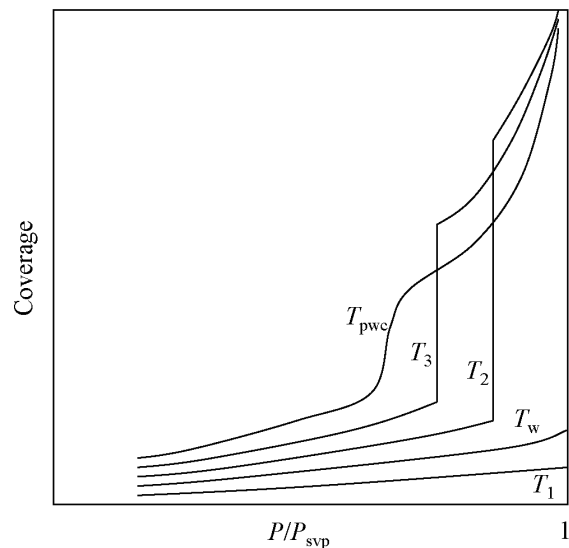


FIG. 1: Schematic diagram of adsorption isotherms near a wetting transition. $T_{pwc} > T_3 > T_2 > T_w > T_1$.

tinuously and the prewetting transition disappears. A schematic diagram showing these three types of adsorption patterns is given in FIG. 1.

Since the first theory on wetting transition was developed a variety of experimental [3–16] and theoretical studies [17–29] have been performed on the wetting transition of fluids on various solid surfaces. Most of these studies were focused on simple fluids such as He and H₂ isotopes on alkali metal surfaces. One common feature of these systems is that the fluid-surface interaction is only weakly attractive. This implies that the bead-up of fluid on the surface at P_{svp} will be favorable over the continuous growth of a film.

Finn and Monson [18] were among the first to calculate the wetting temperature of fluid on solid sur-

*Electronic address: xiongce.zhao@nih.gov

[†]Current address: NIDDK, National Institutes of Health, Bethesda, MD 20892, USA

face using molecular simulations. They predicted the wetting behavior of Ar on solid CO₂ surface using isobaric-isothermal Monte Carlo simulations. Shi *et al.* [30] reevaluated this system using grand canonical Monte Carlo (GCMC) simulations plus multiple histogram reweighting techniques. Errington [31] studied the same system by employing a new simulation method. Bojan *et al.* [25] studied wetting behavior of Ne on surfaces with various interaction strengths. Curtarolo *et al.* [26] used GCMC simulations to study the wetting behavior of inert gases on alkali and Mg surfaces. Shi *et al.* [28] studied the wetting transition of hydrogen isotopes on Rb surface by including the quantum effects of the fluids using path integral hybrid Monte Carlo simulations.

The wetting transition of fluid-fluid systems were studied by both experiments and theory, [32] but the wetting behavior of fluids on solid surfaces was only reported for atomistic molecules such as inert gases. No wetting transition has ever been seen for any molecular fluids on solids other than hydrogen and its isotopes, which are essentially spherical molecules. To our knowledge, the wetting transition involving water has not been studied until very recently [29] although water is an extensively studied molecule. It is known that water does not wet many surfaces (such as graphite) at room temperature. Theoretically, the wetting transition of water on graphite is expected to occur at a temperature below its bulk critical temperature. In a recent paper by Gatica *et al.*, [29] wetting temperatures of water on graphite had been predicted using a simple model based on the water-solid interaction calculated from empirical potentials. The recommended T_w from their calculations for water on graphite is 474 K.

In this study, we report evidence for the first-order wetting transition of water on graphite from molecular simulations. We estimate the wetting transition temperature and prewetting critical temperature of water on graphite using grand canonical Monte Carlo simulations. The paper is organized as the following: The next section describes the potential models and simulation methodology. Section III presents the results and discussion. Section IV summarizes our findings.

II. POTENTIALS AND METHODS

Water-water interaction is described by the SPC/E model. [33] This model is widely used in modeling systems involving water. The model includes a Lennard-Jones site located on the oxygen atom and three partial charge sites on each atom. The parameters for this model are given in TABLE I. The critical temperature of water calculated using the SPC/E model is 635 K. [34] This value is the closest to the experimental value (647 K) compared with the predictions by many other popular nonpolarizable water potentials. [35] Up to date there is no potential available being able to reproduce in every detail the properties of real water. [35] It is known

that the ability of an interaction potential to describe the bulk critical behavior is a necessary (though not sufficient) requirement in order for it to predict the wetting transition behavior of the fluid on a surface. [32] Therefore, we chose the SPC/E model among tens of water potentials available.

The graphite surface is modeled as a smooth basal plane. The Lennard-Jones interaction between a water molecule and the graphite surface is given by the 10-4-3 potential [36]

$$V_{\text{sfLJ}}(z) = 2\pi\epsilon_{\text{sf}}\sigma_{\text{sf}}^2\Delta\rho_{\text{s}}\left[\frac{2}{5}\left(\frac{\sigma_{\text{sf}}}{z}\right)^{10} - \left(\frac{\sigma_{\text{sf}}}{z}\right)^4 - \frac{\sigma_{\text{sf}}^4}{3\Delta(0.61\Delta + z)^3}\right], \quad (1)$$

where z is the distance between the oxygen atom in a water molecule and the graphite surface in the surface normal direction, σ_{s} is the number density of carbon atoms in graphite, and Δ is the distance between the graphene sheets in graphite. The graphite surface corrugation is not included in this potential. The graphite-water interaction parameters ϵ_{sf} and σ_{sf} are calculated from the Lorentz-Berthelot rules,

$$\epsilon_{\text{sf}} = (\epsilon_{\text{s}}\epsilon_{\text{f}})^{1/2}, \quad \sigma_{\text{sf}} = (\sigma_{\text{s}} + \sigma_{\text{f}})/2.$$

The values of the parameters are: $\rho_{\text{s}}=114 \text{ nm}^{-3}$, $\Delta=0.335 \text{ nm}$, $\epsilon_{\text{s}}=0.05569 \text{ kcal/mol}$, and $\sigma_{\text{s}}=0.340 \text{ nm}$ for graphite, $\epsilon_{\text{f}} = \epsilon_{\text{O}}=0.1554 \text{ kcal/mol}$, and $\sigma_{\text{f}} = \sigma_{\text{O}}=0.3165 \text{ nm}$ for water.

A recently developed effective potential for the dipole-induced dipole, dipole-quadrupole, and quadrupole-quadrupole interactions between polar fluids and graphite [37] is used to calculate the water-graphite polar interactions. For water/graphite system, only the induction and dipole-quadrupole terms are important,

$$V_{\text{polar}}(z) = -\frac{\pi\Delta\rho_{\text{s}}\mu_{\text{f}}^2}{(4\pi\epsilon_0)^2}\left[\frac{\alpha_{\text{C}}}{2}\left(\frac{1}{z^4} + \frac{1}{3\Delta(\Delta + z)^3}\right) + \frac{\Theta_{\text{C}}^2}{3k_{\text{B}}T}\left(\frac{1}{z^6} + \frac{1}{5\Delta(\Delta + z)^5}\right)\right], \quad (2)$$

where ϵ_0 is the vacuum permittivity, k_{B} is the Boltzmann's constant, μ_{f} is the dipole moment of the water molecule, α_{C} is the isotropic polarizability of a carbon atom in graphite, and Θ_{C} is the permanent quadrupole moment on each carbon atom in graphite. The values for these parameters are $\mu_{\text{f}}=1.85 \text{ Debye}$, $\alpha_{\text{C}} = 1.76 \times 10^{-3} \text{ nm}^3$, [38] and $\Theta_{\text{C}} = -3.03 \times 10^{-40} \text{ C m}^2$. [39] We note that μ_{f} calculated for SPC/E model is 2.07 Debye, but 1.85 Debye is chosen here so that comparison can be made between this study and Gatica *et al.*'s prediction.

Ewald summations were applied in simulations to account for the long-range correction to electrostatic interactions. Since only two dimensional periodic boundary conditions along x and y directions were applied in the

TABLE I: Potential parameters for SPC/E model. [33] r_{OH} is the O-H bond length, θ_{HOH} is the H-O-H bond angle. ε_{O} and σ_{O} are Lennard-Jones parameters for the O atom. q_{O} and q_{H} are the partial charges on O and H atoms, respectively.

$r_{\text{OH}}[\text{nm}]$	θ_{HOH}	$\varepsilon_{\text{O}}[\text{kcal/mol}]$	$\sigma_{\text{O}}[\text{nm}]$	$q_{\text{O}}[e]$	$q_{\text{H}}[e]$
0.1	109.47°	0.1554	0.3165	-0.8476	0.4238

adsorption simulations, a pseudo-two-dimensional Ewald summation method [40] was used. The total electrostatic energy is given by

$$\begin{aligned}
 V_{el} = & \frac{1}{2V_0\varepsilon_0} \sum_{k \neq 0}^{\infty} \frac{e^{-k^2/4\alpha^2}}{k^2} \left| \sum_j^N q_j e^{-i\mathbf{k}\cdot\mathbf{r}_j} \right|^2 \\
 & + \frac{1}{4\pi\varepsilon_0} \left[\sum_{n < j}^N \frac{q_n q_j}{r_{nj}} \text{erfc}(\alpha r_{nj}) \right. \\
 & \left. - \sum_{mole} \left(\frac{\alpha}{\sqrt{\pi}} \sum_{j=1}^{site} q_j^2 + \sum_{n,j}^{list} \frac{q_n q_j}{r_{nj}} \right) \right] + \frac{M_z^2}{2V_0\varepsilon_0}, \quad (3)
 \end{aligned}$$

where V_0 is the volume of the simulation cell and α is the Ewald convergence parameter. In Eq. (3), the first term is the reciprocal sum for all the Gaussian charges, \mathbf{k} is the reciprocal lattice vector, q_j is the partial charge on interacting site j , \mathbf{r}_{nj} is the vector from \mathbf{r}_n to \mathbf{r}_j . The second term is the standard real-space sum, erfc is the complementary error function. The third term is the self-exclusion on each molecule, plus the 1-2 and 1-3 intramolecular exclusions, where *site* is the total number of partial charge sites in the molecule, and *list* contains all the 1-2, 1-3 exclusions. The last term is the 2D correction term, where M_z is the z component of the total dipole moment of the simulation box.

We have used grand canonical Monte Carlo simulations combined with multiple histogram reweighting (MHR) method [41, 42] to compute the saturated coexistence chemical potentials [43] and adsorption isotherms [30] of water on graphite at various temperatures. More details on the MHR method can be found from the original literature [41, 42] and several other articles on its applications. [43, 44] The GCMC cell for adsorption simulations is a rectangular box with volume of $2000\sigma_f^3$. The height of adsorption box in the z direction, H , is $15\sigma_f$, the sides in x and y directions are $11.5\sigma_f$. The lower plane normal to the z axis is modeled as the graphite surface.

Special care was taken to avoid capillary condensation effects on the wetting transition properties of the system. The plane opposite to the graphite surface is modeled as a hard repulsive wall. The hard wall is always dry to the liquid phase and wet to the gas phase. Therefore it helps to suppress the capillary condensation. [18, 45–48] The capillary condensation can also be eliminated by using a simulation cell with sufficient separations between the adsorbent surface and the opposite hard wall. [18, 25, 26, 28] However, an overall

small cell volume is preferred for the MHR technique. Therefore, we have performed series of trial simulations using various cell heights to search for an appropriate value of H . Trial simulations were performed using cell heights ranging from $10\sigma_f$ to $40\sigma_f$ at interested temperatures and chemical potentials (pressures). It was found that the adsorption properties such as isotherms obtained at $15\sigma_f$ are consistent with those obtained at $20\sigma_f$, $30\sigma_f$, and $40\sigma_f$ within the statistical fluctuations (see FIG. 2 for an example). This indicates that $15\sigma_f$ is adequate for effectively avoiding the influence of capillary condensation for the systems of interest. Based on this we chose $15\sigma_f$ as the cell height in most of our GCMC simulations. Additional simulations with $H=20\sigma_f$ were performed as verifications at each temperature.

The type of move to attempt during a GCMC simulation was selected randomly with probability of 0.45, 0.45, 0.05, and 0.05 for displacements, rotations, creations, and deletions of a water molecule, respectively. Each simulation included equilibration of 80×10^6 MC moves and production of 20×10^6 MC moves. Histograms were collected every 20 MC moves during the production. The cutoff of pair-wise Lennard-Jones interaction between water molecules was 0.9 nm as suggested by the original literature, without long-range correction applied. [33]

In the light of Gatica *et al.*'s prediction, [29] we chose to perform GCMC simulations at 460, 470, 480, 490, 500, 510 K with varying reduced chemical potentials to obtain the histograms for bulk water and water/graphite adsorption systems. The values of bulk saturation chemical potentials (μ_{svp}^*) at each different temperature can be determined using the MHR method by combining the histograms collected. The MHR provide very precise values of μ_{svp} through the equal area criterion, [43] which is very important for studying wetting transitions. Sufficient overlap between histograms of adjacent state points is necessary in order to use the MHR technique. We employed the method proposed by Shi *et al.* [30] to check the overlap of any two adjacent state points. According to this method, the grand canonical partition functions extrapolated by histogram reweighting method for any two adjacent state points should approximately satisfy

$$\frac{\Xi(\mu_i, V, T_i)}{\Xi(\mu_j, V, T_j)} \Big|_{\text{HR}} \times \frac{\Xi(\mu_j, V, T_j)}{\Xi(\mu_i, V, T_i)} \Big|_{\text{HR}} = 1 \pm \delta, \quad (4)$$

where the subscript HR indicates that the partition function in the numerator has been extrapolated from the histogram reweighting of the state point in the denominator. The recommended value for δ is 0.65 for checking the overlap of two adjacent state points. [30] Whenever the overlap criterion defined in Eq. (4) is not satisfied by any of two adjacent state points, additional simulations at state points that bridge them were performed. From preliminary simulations we found that the wetting transition of water on graphite occurs approximately between 470 and 480 K and the wetting critical temperature is between 500 and 510 K. In order to narrow down the values of T_w and T_{pwc} , we performed additional simulations at

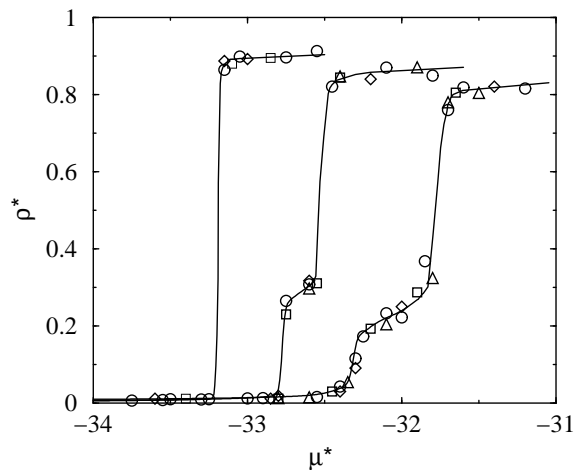


FIG. 2: Typical adsorption isotherms of water on graphite from GCMC simulations and MHR, where ρ^* is the reduced number density and μ^* is the reduced chemical potential. The curves correspond to $T=475, 490, 510$ K, from left to right, which were computed from MHR using histograms collected from simulations with cell height $H=15\sigma_f$. The symbols are data from individual GCMC simulations and were not included in the MHR calculations. Circles: $H=15\sigma_f$, squares: $H=20\sigma_f$, diamonds: $H=30\sigma_f$, triangles: $H=40\sigma_f$.

475 K and 505 K.

III. RESULTS AND DISCUSSIONS

GCMC adsorption simulations were carried out for reduced chemical potentials up to saturation under each selected temperature. Isotherms were calculated using MHR based on the histograms collected during the simulations. Three representative isotherms are plotted in FIG. 2. Some of the data points calculated directly from GCMC simulations but not included in the MHR calculation are also plotted in the figure to compare with isotherms from MHR. It can be seen that the difference between the densities obtained from direction GCMC simulations and those from MHR are small. This serves as a test of the accuracy of the MHR isotherms.

To present the isotherms obtained at different temperatures in a concise and clear fashion, we define a parameter as

$$\chi^* = \exp\left(\frac{\mu^* - \mu_{\text{sVP}}^*}{T^*}\right),$$

where μ^* is the reduced chemical potential, μ_{sVP}^* is the saturation chemical potential at the reduced temperature T^* . Plotting the adsorption coverage versus χ^* gives a diagram similar to FIG. 1, which helps one to identify the wetting transition points without ambiguity. The parameter χ^* is the ratio of the activity to the activity at saturation, with $\chi^* = 1$ corresponding to $\mu = \mu_{\text{sVP}}^*$, or $P = P_{\text{sVP}}$. Additionally, $\chi^* = P/P_{\text{sVP}}$ if ideal behavior is

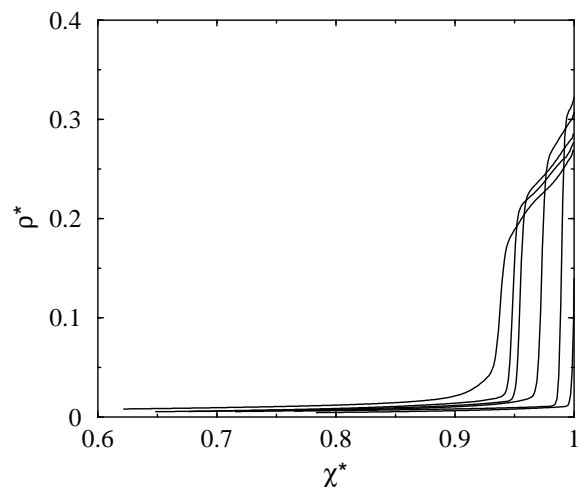


FIG. 3: Adsorption isotherms of water on graphite from GCMC simulations and MHR. The curves correspond to $T=510, 505, 500, 490, 480, 475$ K, from left to right.

assumed in the bulk vapor phase. However, water vapor cannot be treated as an ideal gas under the interested simulation temperatures in this study. For example, the experimental compressibility factor of the saturated water vapor is about 0.865 [49] at 500 K.

As the chemical potential was increased toward saturation, three different types of behavior in the growth of the water adsorption film on graphite were observed, corresponding to three ranges of temperature. Adsorption isotherms for water/graphite at several representative temperatures are shown in FIG. 3.

At temperatures below 475 K, the adsorption coverage is minuscule until the saturation chemical potential is reached, which indicates partial wetting or non-wetting. The isotherm jumps to the saturated liquid density at χ_{sVP}^* , which can be seen from FIGs. 2, 3, and from the density profile growth patterns shown in FIG. 4. The sharp increase of density between $\chi^*=0.991$ and $\chi^*=1.008$ corresponds to a first-order transition from nonwetting to liquid condensation (FIG. 4). At $\chi^*=1.008$, much of the density profile becomes comparable with the saturated liquid density profile (the saturated liquid density at 475 K is $\rho^* \approx 0.89$ from bulk GCMC simulations) except for the first peak corresponds to the density of liquid film in contact with the wall.

In contrast, the simulation results at temperatures between 480 K and 505 K manifest quite different behavior. Taking the isotherm at 490 K as an example, there is sudden jump in adsorption from minimum to a finite coverage of about $\rho^*=0.25$ at $\chi^*=0.965$ to $\chi^*=0.972$ (FIG. 5). But apparently the increased coverage does not correspond to a liquid condensation (the saturated liquid density at 490 K is $\rho^* \approx 0.85$). As the chemical potential is increased further, the film thickens, which indicates a wetting behavior (FIGs. 2, 3, 5). By comparing the results shown in FIG. 3 and FIG. 1 we readily see that

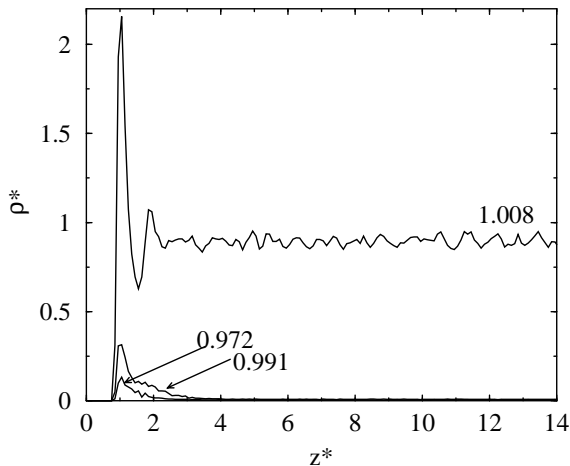


FIG. 4: The local density profiles for water adsorption on graphite as a function of reduced distance from the surface, $z^* = z/\sigma_f$, at 475 K. The values of χ^* at which the calculations were performed are indicated by the labels in the graph.

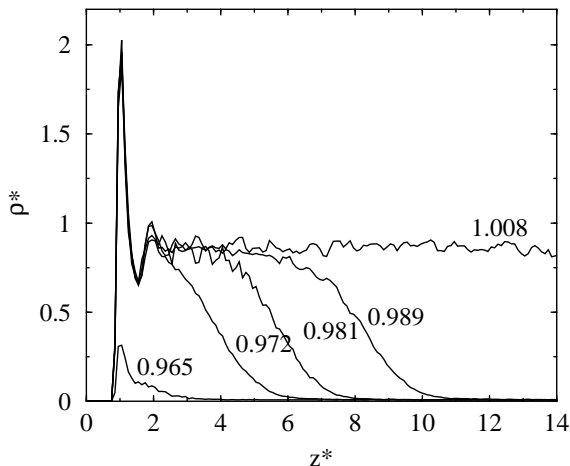


FIG. 5: The local density profiles for water on graphite as a function of reduced distance from the surface at 490 K. The values of χ^* at which the calculations were performed are indicated by the labels in the graph.

wetting transition of water on graphite occurs somewhere between 475 K and 480 K, i. e., $T_w=475-480$ K. At temperatures in the range of 480 K and 505 K, the prewetting jump in density occurs further to the saturation chemical potential with the smaller density jump as temperature increases (FIG. 3).

At $T=510$ K, the adsorption isotherm becomes continuous as the chemical potential increases (FIG. 3), which indicates $T_{pwc} \leq 510$ K. This is more clearly presented by the growth of density profiles shown in FIG. 6. The adsorption film builds from a thin to a thick one continuously with the increase of the chemical potential. The density of the first peak in the profiles increases gradually to that of an adsorbed liquid. At saturation chemical po-

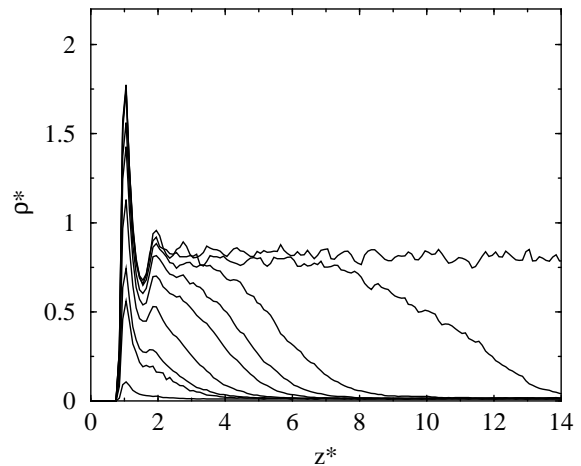


FIG. 6: The local density profiles for water on graphite as a function of reduced distance from the surface at 510 K. Profile curves are for $\chi^* = 0.731, 0.878, 0.892, 0.919, 0.940, 0.962, 0.977, 0.995, 1.003$, from bottom to top.

tential, the density profile evolves to the one corresponding to the liquid density except for the first peak adjacent to the wall. Comparison of the isotherms obtained at 505 K and 510 K in FIG. 3 with FIG. 1 indicates that the prewetting critical temperature of water on graphite lies somewhere between these two values of temperature, i.e. $T_{pwc}=505-510$ K.

The nature of the prewetting jump of water on graphite at temperatures 480- 505 K can be further shown by the results obtained from simulations at 490 K, $\chi^* = 0.992$, with varying simulation cell dimension in the surface normal direction. Shown in FIG. 7 are the density profiles obtained from simulations with cell heights of $H^* = h/\sigma_f = 10, 20, 30, 40$, respectively. In order to compare the results with consistency, in those four simulations the area of the graphite wall is kept at $10\sigma_f \times 10\sigma_f$, but the height, or the volume, of the cell varies. It can be seen from FIG. 7 that the rapid rise of the film thickness to a finite value is independent of the height of the simulation cell. The film thickness keeps at about $7.5\sigma_f$ under various H^* . This is a clear indication that the transition is prewetting rather than capillary condensation. We also notice that the density profile at $H^*=10$ has more fluctuations compared with those at $H^*=20, 30$, and 40. That could be due to the finite size effects in H^* . This confirms the importance of using a simulation cell with sufficient height in order to obtain reliable wetting transition information. Theoretically the density profiles obtained with different H^* should coincide with each other. But it is hard to achieve this in simulations because of statistical fluctuations and metastability nature of the problem.

One of the clearest demonstrations of the first-order nature of many wetting transitions is the observation of one stable and one metastable states shown in the systems of interest in the temperature range of T_w to T_{pwc} [32]. The experimental work by Bonn *et al.* [50]

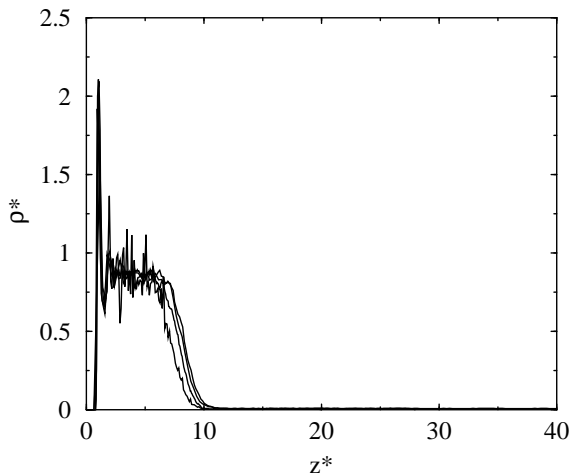


FIG. 7: Film density for water on graphite at $T=490$ K and $\chi^* = 0.992$. Curves correspond to varying heights of the simulation cell: $H^* = 10, 20, 40, 30$, from left to right.

showed that two different stable values of the film thickness could be found in the binary liquid mixture of methanol/cyclohexane at a temperature between 295 K and 308 K. The thin film of 1.0 nm is the metastable state, and the thick film of 40.0 nm is the stable state. Shi *et al.* [28] observed the similar switching behavior between thin and thick films in the simulation study of hydrogen isotopes on alkali metal surfaces.

We also observed the coexistence of stable and metastable states for water on graphite, which is shown in FIG. 8. The probability density function of the water density distribution in the box is collected during the simulation with $T=490$ K, $\chi^* = 0.968$. One major peak is located at $\rho^* \approx 0.012$ corresponding to a thin film, at which the simulation samples most frequently. Another small peak exists at $\rho^* \approx 0.25$, which corresponds to a thick film. The bimodal feature of the probability density function of the distribution indicates the wetting transition at this temperature is first order. The switching between the thin and thick films is further confirmed by the fluctuation of the number density of adsorbate in the box. In the inset of FIG. 8 we show the evolution of water density in the simulation cell as a function of simulation steps. At about 11×10^6 configurations the system abruptly jumps to a higher density of $\rho^* \approx 0.25$ from $\rho^* \approx 0.012$, corresponding to a switching from thin film to thick film. This thick film subsequently evaporates to the thin film at about 14×10^6 configurations. Comparing the sizes of the two peaks and evolution of the number density fluctuation we readily conclude that at this state point, the thin film is stable and the thick film was metastable.

In this work we did not attempt to determine the exact values of the wetting temperature or the prewetting critical temperature, but only provide estimated ranges for them, which are 475-480 K and 505-510 K, respectively.

One reason is the lack of reliable theoretical method for determination of exact T_w and T_{pwc} . One of the popular techniques being used previously is a power law extrapolation method [24]. Theoretical predictions indicate that $\Delta\mu^* = (\mu_{sv}^* - \mu_w^*) \propto (T^* - T_w^*)^{3/2}$ [24]. Hence, a plot of $\Delta\mu^*$ versus T^* can be used to identify T_w^* by extrapolating the curve to $\Delta\mu^* = 0$ [3], with the saturation and wetting transition chemical potentials (μ_{sv}^* and μ_w^*) at various temperatures up to T_c of the fluid being calculated from MHR. However, Shi *et al.* [30] found that this power law extrapolation method could be quite inaccurate in predicting the wetting temperature of certain system.

Another important concern is the realism of the water potential employed in this study. It is known that the transition temperature calculated from simulations is sensitively dependent on the solid-fluid interactions [26, 28]. For example, Shi *et al.* found that a $\sim 10\%$ increase in the surface-fluid attraction decreases the wetting transition temperature of Ar on a CO_2 surface by 3 K [28]. In this work, the choice of the water potential will affect the graphite-water interaction implicitly, and thus the calculated T_w . The SPC/E water potential gives by far the best predictions for the critical properties of the bulk water among all the available nonpolarizable water models, while it still cannot simulate exactly the coexistence properties of real water. The accuracy of the estimated T_w and T_{pwc} may be improved by using more accurate polarizable models such as the Gaussian charge polarizable model [51].

In addition, by modeling the graphite as a smooth surface, we neglected the possible impact from surface corrugations and dynamics of the surface structure during the adsorption. A previous simulation work indicates that impact of surface corrugation of the adsorbent on the wetting transition behavior of Ne is minimal [25]. But it is unclear if the same conclusion is applicable to the graphite-water system.

Cheng *et al.* [20] proposed a simple model (CCST hereafter) which interprets the wetting transitions in terms of a balance between the surface tension cost of producing a thicker film and the energy gain associated with the film's interaction with the surface, $V(z)$. The theory results in an implicit equation for the wetting temperature

$$I = - \int_{z_{\min}}^{\infty} V(z) dz = \left(\frac{2\gamma}{\rho_l - \rho_v} \right)_{T_w}, \quad (5)$$

where ρ_l and ρ_v are the number densities of the adsorbate liquid and vapor at coexistence, γ is the surface tension of the liquid, and z_{\min} minimizes the fluid-surface interaction potential $V(z)$. The wetting transition temperature can be calculated by solving the equation since the right hand side of Eq. (5) is dependent implicitly on temperature. The impact of solid-fluid interaction on T_w is reflected by I , and the fluid-fluid interaction is incorporated in the model by γ and $\rho_l - \rho_v$.

The wetting transition of water on graphite calculated in this work agree quantitatively with the previous pre-

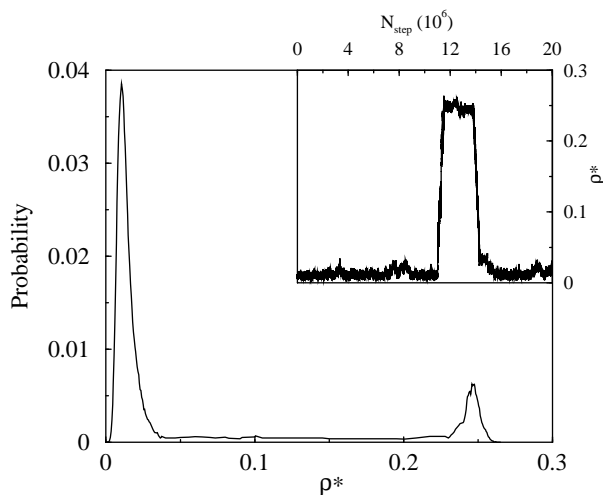


FIG. 8: The switching between the thin and thick film of water adsorption on graphite at $T=490$ K, $\chi^* = 0.968$. The inset shows the density evolution during the simulation.

diction [29] using the CCST model, although different water potentials are employed in the two studies. It has been pointed out by Shi *et al.* [28] that the wetting behavior predicted theoretically depends on both the well depth and well shape of the solid-fluid interacting potential. Here the potential width is defined as the full width at half minimum of the attractive part of the potential. In Gatica *et al.*'s work, TIP4P was used instead of SPC/E. But we note that the well depth (D) and well width (w) of the water/graphite potential for SPC/E and TIP4P are almost identical, both with $D = 9.35$ kJ/mol and $w = 0.135$ nm, if evaluated at $T = 475$ K and using the water dipole moment of 1.85 D. Therefore we expect that the wetting transition temperature calculated from the CCST model using these two potentials be comparable. If the simulation results in this work are taken to be standard, the CCST model predicted T_w of 474 K is very accurate indeed. It has been shown that the CCST model usually works well in predicting the wetting behavior in-

volving spherical fluids such as inert gases, but it has not been tested extensively with nonspherical molecules. The fact that this simple model works well in predicting the wetting of water on graphite, although water has a very different kind of potential than inert gases, indicates that the CCST model contains the essential physics of wetting.

IV. CONCLUSIONS

In summary, we report the first simulation study of the wetting transition of water on graphite surface. The wetting transition temperature calculated from GCMC simulations is 475-480 K, and the prewetting critical temperature is 505-510 K. The wetting transition is first order. The simulation results in this work agrees well with the prediction by the CCST model, although the CCST model is designed on the basis of the simple fluids such as inert gases.

Finally, we point out that the wetting temperature and prewetting critical temperature calculated in this work depends on the accuracy of the water potential employed. Improvement in the predictions may be made if more accurate water potential is available. Future investigations can be performed by including the corrugation of graphite surface, the finite size effect of the system, and by using the more robust simulation techniques such as the one proposed by Errington [31]. Experimental search for the predicted wetting behavior is also warranted.

Acknowledgments

The author thanks Peter T. Cummings and Milton W. Cole for many helpful discussions throughout this work. This research was conducted at the Center for Nanophase Materials Sciences, which is sponsored at Oak Ridge National Laboratory by the Division of Scientific User Facilities, U.S. Department of Energy.

-
- [1] J. W. Cahn, *J. Chem. Phys.* **66**, 3667 (1977).
 - [2] C. Ebner and W. F. Saam, *Phys. Rev. Lett.* **38**, 1486 (1977).
 - [3] G. Mistura, H. C. Lee, and M. H. W. Chan, *J. Low Temp. Phys.* **96**, 221 (1994).
 - [4] D. Ross, P. Taborek, and J. E. Rutledge, *Phys. Rev. Lett.* **74**, 4483 (1995).
 - [5] R. B. Hallock, *J. Low Temp. Phys.* **101**, 31 (1995).
 - [6] B. Demolder, N. Bigelow, P. Nacher, and J. Dupont-Roc, *J. Low Temp. Phys.* **98**, 91 (1995).
 - [7] A. F. G. Wyatt, J. Klier, and P. Stefanyi, *Phys. Rev. Lett.* **74**, 1151 (1995).
 - [8] M. Yao and F. Hensel, *J. Phys.: Condens. Matter* **8**, 9547 (1996).
 - [9] G. B. Hess, M. J. Sabatini, and M. H. W. Chan, *Phys. Rev. Lett.* **78**, 1739 (1997).
 - [10] D. Ross, J. A. Phillips, J. E. Rutledge, and P. Taborek, *J. Low. Temp. Phys.* **106**, 81 (1997).
 - [11] V. F. Kozhevnikov, D. I. Arnold, S. P. Naurzakov, and M. E. Fisher, *Phys. Rev. Lett.* **78**, 1735 (1997).
 - [12] D. Ross, P. Taborek, and J. E. Rutledge, *Phys. Rev. B* **58**, R4274 (1998).
 - [13] F. Hensel and M. Yao, *Ber-Bunsen-Ges. Phys. Chem.* **102**, 1798 (1998).
 - [14] Y. Ohmasa, Y. Kajihara, and M. Yao, *J. Phys.: Condens. Matter* **10**, 11589 (1998).
 - [15] Y. Ohmasa, Y. Kajihara, and M. Yao, *Phys. Rev. E* **63**, 051601 (2001).
 - [16] V. F. Kozhevnikov, D. I. Arnold, S. P. Naurzakov, and M. E. Fisher, *Fluid Phase Equilib.* **150**, 625 (1998).

- [17] C. Ebner and W. F. Saam, Phys. Rev. B **35**, 1822 (1987).
- [18] J. E. Finn and P. A. Monson, Phys. Rev. A **39**, 6402 (1989).
- [19] E. Cheng, M. W. Cole, W. F. Saam, and J. Treiner, Phys. Rev. Lett. **67**, 1007 (1991).
- [20] E. Cheng, M. W. Cole, W. F. Saam, and J. Treiner, Phys. Rev. B **48**, 18214 (1993).
- [21] M. Wagner and D. M. Ceperley, J. Low. Temp. Phys. **94**, 185 (1994).
- [22] M. J. Bojan, M. W. Cole, J. K. Johnson, W. A. Steele, and Q. Wang, J. Low Temp. Phys. **110**, 653 (1998).
- [23] M. Boninsegni and M. W. Cole, J. Low Temp. Phys. **110**, 685 (1998).
- [24] F. Ancilotto and F. Toigo, Phys. Rev. B **60**, 9019 (1999).
- [25] M. J. Bojan, G. Stan, S. Curtarolo, W. A. Steele, and M. W. Cole, Phys. Rev. E **59**, 864 (1999).
- [26] S. Curtarolo, G. Stan, M. J. Bojan, M. W. Cole, and W. A. Steele, Phys. Rev. E **61**, 1670 (2000).
- [27] F. Ancilotto, S. Curtarolo, F. Toigo, and M. W. Cole, Phys. Rev. Lett. **87**, 206103 (2001).
- [28] W. Shi, J. K. Johnson, and M. W. Cole, Phys. Rev. B **68**, 125401 (2003).
- [29] S. M. Gatica, J. K. Johnson, X. C. Zhao, and M. W. Cole, J. Phys. Chem. B **108**, 11704 (2004).
- [30] W. Shi, X. C. Zhao, and J. K. Johnson, Mol. Phys. **100**, 2139 (2002).
- [31] J. R. Errington, Langmuir **20**, 3798 (2004).
- [32] D. Bonn and D. Ross, Rep. Prog. Phys. **64**, 1085 (2001).
- [33] H. J. C. Berendsen, J. R. Grigera, and T. P. Straatsma, J. Phys. Chem. **91**, 6269 (1987).
- [34] T. M. Hayward and I. M. Svishchev, Fluid Phase Equilib. **182**, 65 (2001).
- [35] B. Guillot, J. Mole. Liquids **101**, 219 (2002).
- [36] W. A. Steele, Surf. Sci. **36**, 317 (1973).
- [37] X. C. Zhao and J. K. Johnson, Mol. Sim. **31**, 1 (2005).
- [38] T. M. Miller and B. Bederson, in *Advances in Atomic and Molecular Physics*, edited by D. R. Bates and B. Bederson (Academic Press, London, 1978), vol. 13, p. 1.
- [39] D. B. Whitehouse and A. D. Buckingham, J. Chem. Soc. Faraday Trans. **89**, 1909 (1993).
- [40] I. C. Yeh and M. L. Berkowitz, J. Chem. Phys. **111**, 3155 (1999).
- [41] A. M. Ferrenberg and R. H. Swendsen, Phys. Rev. Lett. **61**, 2635 (1988).
- [42] A. M. Ferrenberg and R. H. Swendsen, Phys. Rev. Lett. **63**, 1195 (1989).
- [43] W. Shi and J. K. Johnson, Fluid Phase Equilib. **187**, 171 (2001).
- [44] J. J. de Pablo, Q. L. Yan, and F. A. Escobedo, Annu. Rev. Phys. Chem. **50**, 377 (1999).
- [45] R. Evans and U. Marini Bettolo Marconi, Phys. Rev. A. **32**, 3817 (1985).
- [46] F. van Swol and J. R. Henderson, J. Chem. Soc. Faraday Trans. II **82**, 1685 (1986).
- [47] A. O. Parry and R. Evans, Phys. Rev. Lett. **64**, 439 (1990).
- [48] A. O. Parry and R. Evans, Physica A **181**, 250 (1992).
- [49] J. M. Smith, H. C. van Ness, and M. M. Abbott, *Introduction to Chemical Engineering Thermodynamics* (McGraw-Hill, New York, 2001), 6th ed.
- [50] D. Bonn, H. Kellay, and G. H. Wegdam, Phys. Rev. Lett. **69**, 1975 (1992).
- [51] P. Paricaud, M. Predota, A. A. Chialvo, and P. T. Cummings, J. Chem. Phys. **122**, 4511 (2005).